LASER INTERFEROMETER GRAVITATIONAL WAVE OBSERVATORY

- LIGO -

CALIFORNIA INSTITUTE OF TECHNOLOGY

MASSACHUSETTS INSTITUTE OF TECHNOLOGY

Document Type	**LIGO-T000000-00-D**	June 20th, 2002

Input Test Mass (ITM) Absolute Calibrations: *Fringe Counting*, *Fringe Fitting*, and *Sign Toggling* Methods

L. Matone, R. Adhikari, M. Evans, M. Landry, S. Marka, H. Yamamoto

Distribution of this draft:
TBD

This is an internal working note
of the LIGO Project.

California Institute of Technology
LIGO Project - MS 18-34
Pasadena, CA 91125
Phone (626) 395-2129
Fax (626) 304-9834
E-mail: info@ligo.caltech.edu

Massachusetts Institute of Technology
LIGO Project - MS 20B-145
Cambridge, MA 01239
Phone (617) 253-4824
Fax (617) 253-7014
E-mail: info@ligo.mit.edu

WWW:http//www.ligo.caltech.edu/

Contents

1 Introduction

The absolute calibration of the Input Test Masses (ITMs) is one of the first steps in calibrating the interferometer strain signal. The goal is to determine the ratio, at DC, of the ITM's displacement to the excitation signal that generated the motion. To measure this ratio, we have investigated three methods that use the input laser wavelength λ as our reference: *Fringe Counting*, *Fringe Fitting* and *Sign Toggling*.

The three approaches present different advantages and disadvantages. The *Fringe Counting* approach is well suited for a quick 5-10% calibration accuracy. However, if an accuracy of $< 5\%$ is desired[1], then the *Fringe Fitting* and *Sign Toggling* methods are more appropriate.

The methods in question have been investigated both numerically (End-to-end[2], LIGO's simulation engine) and experimentally on the 4 km baseline LIGO interferometer (IFO) at Hanford (WA). We present, in this note, the results of the investigation.

2 Fringe Counting

The idea behind *Fringe Counting* is to compare the drive signal sent to one mirror to the number of fringes seen by the Anti-Symmetric (ASY) port output, with the IFO in the simple Michelson configuration and the masses free swinging. The calibration is obtained by comparing the number of fringes crossed to the drive change, with each bright-fringe-to-bright-fringe crossing corresponding to $\lambda/2$ and assuming the ITM's motion to be dominated by the drive.

This approach is certainly appropriate for 5-10% calibrations. If the $< 5\%$ level is desired, however, the mechanical TF of the suspension must also be known with the same degree of accuracy. This is caused by a limit on the drive frequency: the lowest practical frequency suited for the measurement is 100mHz.

If the transfer function in question is not known to the same degree of accuracy, a series of systematic contributions cannot be taken into account in the data analysis. First, driving at 100mHz causes an effective amplification of the drive (contributing to approximately a 2% bias) due to the suspension fundamental mode at 740mHz. Secondly, for the suspension in question, the mirror position phase lags the 100mHz drive (typically by about 1 deg) generating a second systematic source of error.

3 Fringe Fitting

An alternative approach to Fringe Counting is *Fringe Fitting*, where the ASY data channel produced by the Fringe Counting method is fit to determine the calibration factor.

In the stationary plane-wave approximation, we can write the power $P(t)$ seen by the photodetector as a function of the cavity length $l_-(t)$ in the form

$$P(t) = A\ \sin^2\left[k\ l_-(t) + \phi\right] + n(t) \tag{1}$$

with the restriction that

$$l_-(t) = B\ \sin(t\ 2\ \pi\ 100mHz) + s(t) \tag{2}$$

where A is an arbitrary scaling factor, k is the wavelength number, ϕ is an arbitrary phase offset, $n(t)$ is a noise term arising from the electronics, B is the amplitude of the injected 100mHz line and it is the calibration factor we are seeking, and s(t) is the seismic component of $l_-(t)$. The algorithm finds the B and $s(t)$ terms that minimize χ^2.

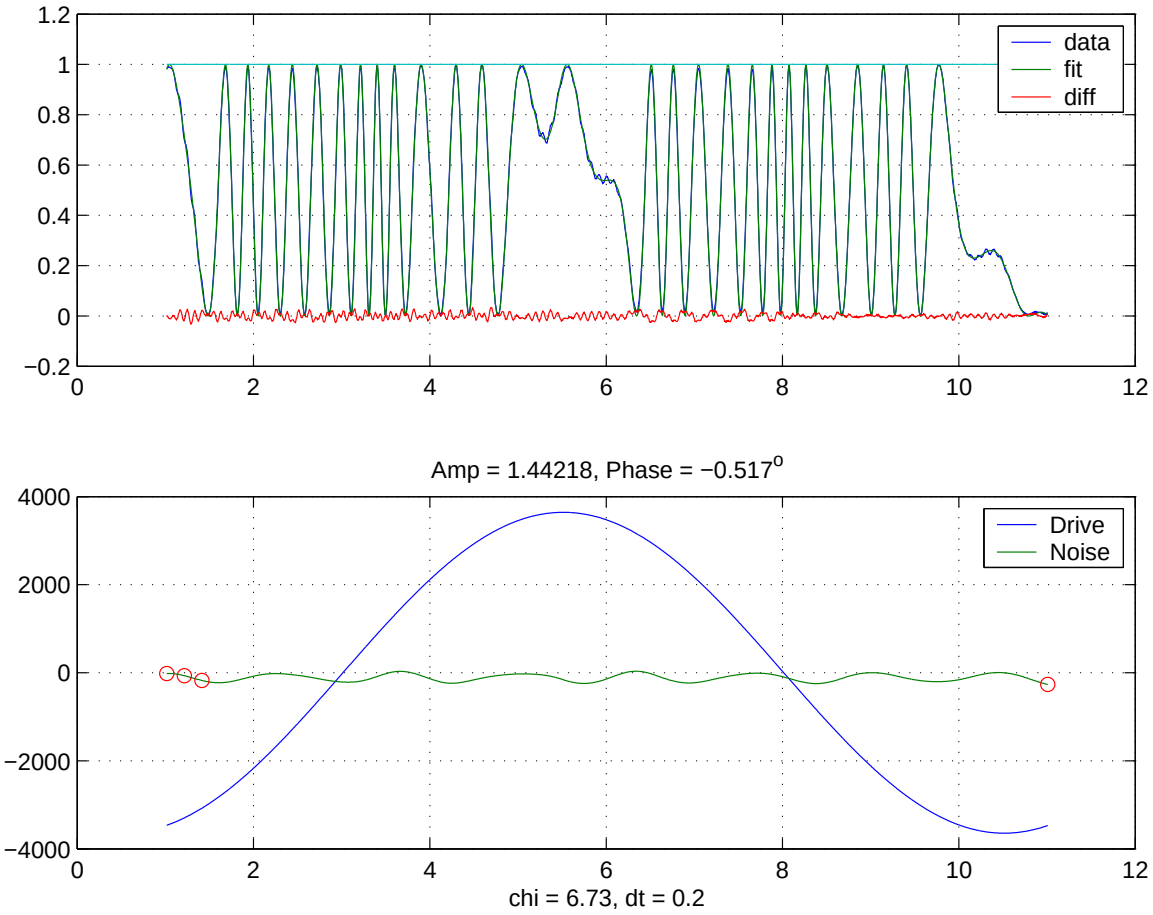

Figure 1: A 10s data stretch of $P(t)$ analysed by the *Fringe Fitting* algorithm. The blue line, on the top graph, is the (normalized) measured photodiode DC power $P(t)$ plotted as a function of time. The green line is the power $P(t)$ generated by the $l_{-}(t)$ found by the algorithm while the red line shows the residual between the two curves. The bottom figure plots the two components of $l_{-}(t)$, $s(t)$ and the harmonic at 100mHz, found by the algorithm.

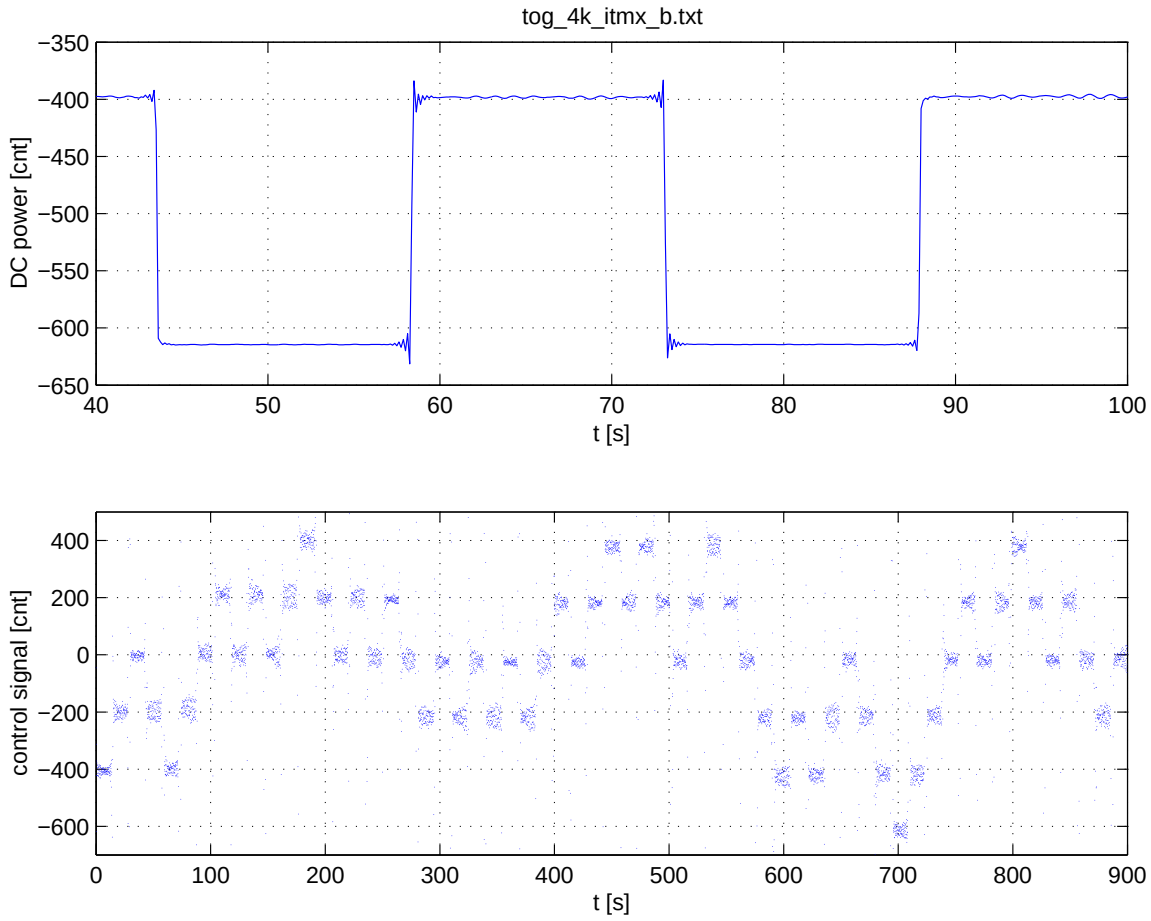

Figure 2: Trend data from the ASY photodetector once the algorithm is enabled. The top graph plots the DC power $P(t)$ as a function of time with the sign of the controller changing every 10s. The bottom graph of fig.(2) plots the correction signal with each cluster of points corresponding to a 10s lock stretch.

Fig.(1) shows the results of the algorithm on 10s of data. The blue line, on the top graph, is the (normalized) measured photodiode DC power $P(t)$ plotted as a function of time. The green line is the power $P(t)$ generated by the $l_{-}(t)$ found by the algorithm while the red line shows the residual between the two curves. On the bottom plot, the two components of $l_{-}(t)$, $s(t)$ and the harmonic at 100mHz, are shown. Generally, the algorithm gives normalized χ^2 values of about < 10, yielding precise calibration factors.

4 Sign Toggling

A different calibration approach was investigated to verify the results of the Fringe Fitting algorithm. The idea behind this method, referred to as *Sign Toggling*, is to lock the IFO in the simple Michelson configuration in dark (bright) fringe and *toggle* the sign of the controller so as to force the system to transition to bright (dark) fringe. Since the transition corresponds to a $\lambda/4$ jump, it is then possible to calibrate the control signal by comparing its level change to $\lambda/4$.

Fig.(2) plots trend data from the ASY photodetector once the algorithm is enabled. The top graph plots the DC power $P(t)$ as a function of time with the sign of the controller changing every

10s. The bright and dark light levels are visible and the reader can verify how the transitions correpond to $\lambda/4$ jumps.

The bottom graph of fig.(2) plots the correction signal as a function of time with each cluster of points corresponding to a 10s lock stretch. The algorithm takes the difference between the different signal levels and determines the calibration factor.

5 Data Analysis

The methods presented in the previous sections aim at determining the absolute calibration of the ITMs at DC. It is necessary, however, to clarify a few points in order to correctly interpret the results of the algorithms.

5.1 Fringe Fitting

When the interferometer is in detection mode, the masses are controlled by small fractions of λ and the calibration procedure should really excite the masses by the same fraction of λ. This is not the case for both procedures under investigation. In particular, the *Fringe Fitting* algorithm has been used on data produced by swinging the ITM by several λ, resulting in a calibration that may well be affected by any non-linearities present in the drive.

On the other hand, this approach presents the advantage of being insensitive to any bias present in the channel output. The algorithm looks for the $l_{-}(t)$ necessary to reproduce the fringe pattern observed regardless of any offset present.

There is, however, one bias term that needs to be addressed arising from the suspension pendulum transfer function. The mirror displacement at 100mHz is amplified by the fundamental mode at 740mHz causing an overestimate of the calibration. Since this bias does not strongly depend on the suspension quality factor Q (numerically verified for values ranging from 2 to 50), the calibration factor given by the algorithm needs to be corrected by 1.8%.

5.2 Sign Toggling

As previously described, the change in the control signal level due to sign toggling is compared to $\lambda/4$ to determine the calibration factor. Since the mean of the signal can be measured precisely and the number of transitions can be relatively high, it is possible to achieve precise calibration numbers.

There is a variety of sources for systematic errors that need to be taken into account if $< 5\%$ accuracies are desired. The following sources have been considered:

- the time response of the servo system;
- the gain constraint;
- the signal offsets;
- and filter compensation.

Since we are using two different calibration methods, we need to make sure we calibrate the same signal. It turns out that the signal the Fringe Fitting method calibrates is not identical to the one the Sign Toggling method calibrates: there is a stop band filter in the latter that has a non-unitary gain at DC. By filter compensation, we mean adjusting for the calibration factor obtained with Sign Toggling by 6%.

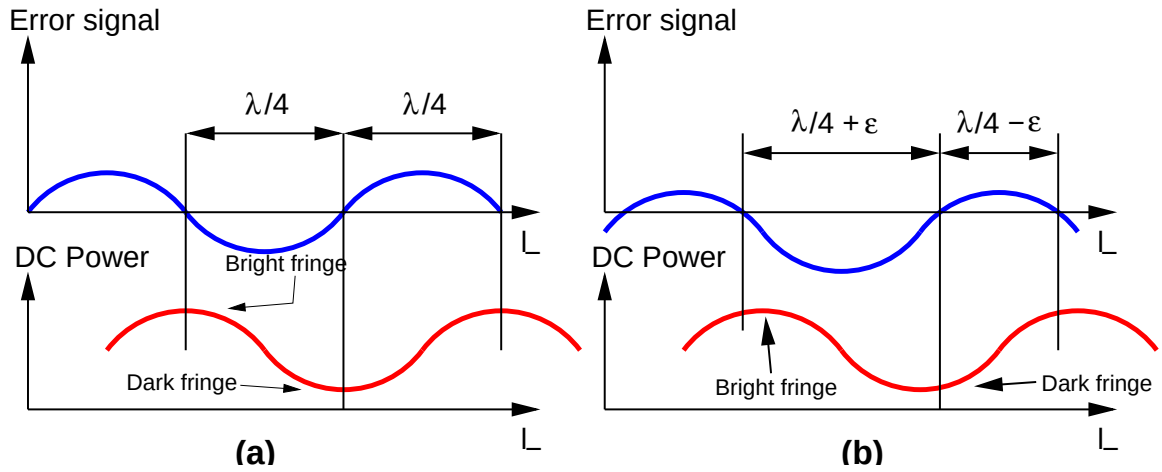

Figure 3: The effect of a bias term in the Sign Toggling approach. On the left, figure illustrating the case of no offset term. The top curve shown is the error/control signal and the bottom one is the DC power seen by ASY photodetector, both plotted as a function of l_-. Locking on dark fringe and transitioning to bright fringe could either expand or contract the cavity length by the same amount $\lambda/4$. On the right, the figure illustrates the case with an offset term. In this case, transitioning to bright fringe exapand and contract the cavity length by $\lambda/4 \pm \epsilon$. This causes different calibration factors for transitions expanding the cavity or contracting the cavity.

5.2.1 Time Response of the Servo System and Gain Constraint

It is necessary to ensure that the system reaches equilibrium before the algorithm analyses the data. To determine this settling time, we represented the system in Matlab with a series of transfer functions (TFs) and we numerically computed its impulse response. For the setup in question, the system reaches equilibrium after a 3s settling time.

Another requirement is on the loop gain G of the system in question. If the Michelson is locked such that the ITM is at its rest position (minimum of the gravitational potential), there would be no recoiling force the servo needs to contrast. In practice, this will hardly be the case, especially if the cavity length changes by $\lambda/4$ steps. For calibration accuracies of $< 5\%$, the constraint on the gain of the system must be

$$\frac{1}{G} << 5\% \tag{3}$$

5.2.2 Offsets

The presence of offsets in the signal chain will introduce a bias term in the calibration as shown in fig.(3). Fig.(3a) illustrates the case in the absence of a bias where the top curve is the error/control signal and the bottom one is the DC power seen by ASY photodetector, both plotted as a function of l_-. If the system is locked on dark fringe, transitioning to the next brigth fringe would either increase or decrease the cavity length by $\lambda/4$. Either transition would displace the cavity length by the same amount.

In the presence of offsets, fig.(3b) shows how the calibration is affected. Since the bias term forces the system to lock not exactly on destructive/constructive interference, transitioning from dark to bright fringe would change the cavity length by $\lambda/4 \pm \epsilon$, where the sign depends on whether the length increases or decreases. Therefore, the transitions expanding the cavity length would yield a different calibration factor from the transitions contracting the cavity length.

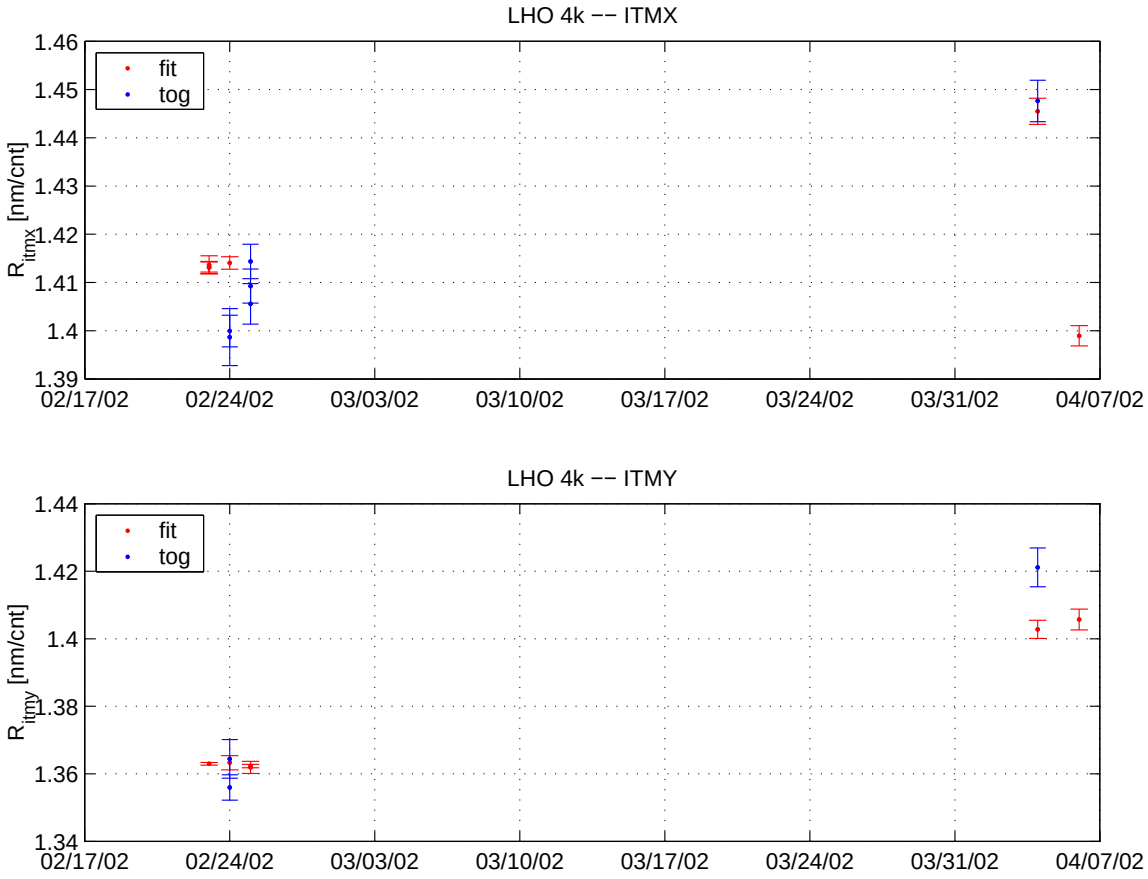

Figure 4:

To get around this problem, the algorithm selects the transitions expanding the cavity length from the ones contracting it. The change the control signal undergoes from the two transitions is then recorded and summed: the sum would then correspond to a $\lambda/2$ transition insensitive to any offset present.

6 Results

In February and April 2002, we tested these methods on the 4km long IFO at Hanford (WA) and the results, after the various adjustements previously discussed, are shown in fig.(4). The top graph shows the absolute calibration for ITMx, the bottom graph for ITMy, in red are the reults from Sign Toggling and in blue from the Fringe Fitting algorithm. The agreement of each approach is within the 1% level wheras the agreement between the approaches is at the $1-2\%$ level.

7 Conclusion

Three different approaches for the absolute calibration of the ITMs have been presented in this letter. The advantages and disadvantages of each have been discussed and a list of systematic errors have been addressed. The methods have been tested numerically with Matlab and e2e and

demonstrated on the 4km long interferometer at Hanford (WA).

The methods have presented promising results, with an agreement for either approach at the 1% level and an agreement between the approaches of $1 - 2\%$.

References

[1] LIGO-T980068-00-D "Length Sensing and Control Subsystem Final Design"

[2] LIGO-T970193-00-E "Overview of the end-to-end model"